Check for updates

JGR Atmospheres

RESEARCH ARTICLE
10.1029/2025JD044301

Special Collection:
Observing CO2 from space: A Decade of progress from NASA's Orbiting Carbon Observatories (OCO-2 and OCO-3)

Observational Requirements for Quantifying the Diurnal Cycle of XCO_2 From Space

G. Keppel-Aleks[1], A. D. Torres[1], E. Tatham[2], S. C. Doney[2], M. de Maziere[3], O. Garcia[4], and C. M. Roehl[5]

[1]Department of Climate and Space Sciences and Engineering, University of Michigan, Ann Arbor, MI, USA, [2]Department of Environmental Sciences, University of Virginia, Charlottesville, VA, USA, [3]Royal Belgian Institute for Space Aeronomy, Brussels, Belgium, [4]Izaña Atmospheric Research Center, Agencia Estatal de Meteorología, Santa Cruz de Tenerife, Spain, [5]Division of Geological and Planetary Sciences, California Institute of Technology, Pasadena, CA, USA

Abstract Spatiotemporal variations in atmospheric carbon dioxide (CO_2) provide a means to quantify surface fluxes of carbon over a range of space and timescales. NASA's Orbiting Carbon Observatory-3 (OCO-3), aboard the International Space Station, is the first CO_2-monitoring mission to observe the sunlit portion of the diurnal cycle of total column-averaged CO_2 (X_{CO2}) from space, since OCO-3 collects data at various times of the day. Previous analysis of the climatological diurnal cycle in X_{CO2} measured from a ground-based spectrometer in the Total Carbon Column Observing Network (TCCON) suggests that the X_{CO2} diurnal cycle provides information about local fluxes. Here, we examine the diurnal signal at four TCCON sites spanning the tropics through midlatitudes. The signal is typically less than 1 ppm even at the peak of the growing season. Because relatively sparse OCO-3 data observes a diurnal cycle at a given location only across multiple days, mesoscale transport variations complicate detection of the diurnal signal from the space-based record. We bootstrap the long-term records of TCCON X_{CO2} to quantify the minimum number of OCO-3 observations necessary to infer the climatological diurnal cycle of X_{CO2}, and find that even during the peak growing season, of order 10 observations per daylight hour for each month are required for robust detection. The number of required observations increases outside the growing season when fluxes are weaker. Our results show that dense and long-term observation are required to infer the diurnal cycle from OCO-3 or future CO_2-monitoring satellite missions.

Plain Language Summary Observations of atmospheric carbon dioxide (CO_2) provide information about the exchange of carbon between the atmosphere and the land surface. The variation of CO_2 from morning to night provides information about local fluxes associated with biosphere photosynthesis and respiration, but is difficult to observe because it is so small. We show that to quantify the diurnal change in CO_2 from space, at least 10 observations per hour per month are required during the peak growing season when plants are actively taking up CO_2 from the atmosphere. At other times of the year, more observations are required to detect a smaller signal.

Key Points:

- The diurnal cycle in total column carbon dioxide (X_{CO2}) is less than 1 ppm even during the peak growing season
- Orbiting Carbon Observatory-3 (OCO-3) data are not yet sufficiently dense to quantify the climatological diurnal cycle
- Ground-based data show that at least 10 independent observations per hour per month are required to robustly quantify the diurnal cycle

Supporting Information:

Supporting Information may be found in the online version of this article.

Correspondence to:

G. Keppel-Aleks,
gkeppela@umich.edu

Citation:

Keppel-Aleks, G., Torres, A. D., Tatham, E., Doney, S. C., de Maziere, M., Garcia, O., & Roehl, C. M. (2026). Observational requirements for quantifying the diurnal cycle of XCO_2 from space. *Journal of Geophysical Research: Atmospheres*, *131*, e2025JD044301. https://doi.org/10.1029/2025JD044301

Received 7 MAY 2025
Accepted 15 DEC 2025

Author Contributions:

Conceptualization: G. Keppel-Aleks, S. C. Doney
Data curation: M. de Maziere, O. Garcia, C. M. Roehl
Formal analysis: A. D. Torres, E. Tatham
Funding acquisition: G. Keppel-Aleks
Methodology: G. Keppel-Aleks
Project administration: G. Keppel-Aleks

© 2026. The Author(s).
This is an open access article under the terms of the Creative Commons Attribution License, which permits use, distribution and reproduction in any medium, provided the original work is properly cited.

1. Introduction

The diurnal cycle of ecosystem carbon exchange provides insights into the sensitivity of fluxes to temperature, radiation, and moisture, which can all vary across the daily cycle. Such observations and sensitivities are critical for parameterizing ecosystem models (Braswell et al., 2005). Atmospheric carbon dioxide (CO_2) observations have been used to infer net ecosystem carbon exchange at seasonal and interannual timescales (e.g., Byrne et al., 2023; Gurney et al., 2002; Liu et al., 2017; Peters et al., 2007). This capability, however, is more challenging at the diurnal timescale, as we describe below.

In situ observations of atmospheric CO_2 have been made continuously at some observatories as part of global cooperative sampling networks. While these observations sample the full diurnal cycle, interpretation of in situ CO_2 variations within the boundary layer is complicated by the fact that diurnal fluxes covary with diurnal boundary layer mixing (Denning et al., 1995). During times of strong ecosystem uptake (typically sunny days), boundary layer turbulence is vigorous and high CO_2 air from aloft is mixed into the boundary layer, leading to a positive bias in the mole fraction within the boundary layer compared to its expected value given a boundary layer of constant height (Denning et al., 1999). In contrast, times of day or year with weak vertical mixing tend to coincide with net respiration of CO_2 into the boundary layer, effectively trapping CO_2 released to the atmosphere

21698996, 2026, 1, Downloaded from https://agupubs.onlinelibrary.wiley.com/doi/10.1029/2025JD044301 by Spanish Cochrane National Provision (Ministerio de Sanidad), Wiley Online Library on [03/03/2026]. See the Terms and Conditions (https://onlinelibrary.wiley.com/terms-and-conditions) on Wiley Online Library for rules of use; OA articles are governed by the applicable Creative Commons License

Supervision: G. Keppel-Aleks, S. C. Doney
Writing – original draft: G. Keppel-Aleks
Writing – review & editing: G. Keppel-Aleks, A. D. Torres, E. Tatham, S. C. Doney

within the boundary layer, which again leads to a positive bias in the observed CO_2 mole fraction relative to what would be expected if boundary layer mixing were constant in time. Because near surface vertical mixing is a challenge to simulate in chemical transport models (Schuh & Jacobson, 2023), there is large uncertainty in the relationship between diurnally varying fluxes and surface or tower CO_2 mole fraction observations (Law et al., 2008).

The strategy to observe the total column-averaged CO_2 mole fraction (X_{CO2}) was introduced in part to circumvent the challenge of robust flux inference from surface observations in the context of uncertain vertical mixing. X_{CO2} is usually measured via remote sensing in the near infrared, where molecules of CO_2 in the atmosphere from the surface through the stratosphere absorb sunlight with wavelength specificity. Since 2009, dedicated carbon satellites have retrieved X_{CO2} using reflected solar spectra. GOSAT was launched in 2009 by the Japanese Space Agency (Yokota et al., 2009), followed by GOSAT-2 in 2018 (Isamu et al., 2023), and most recently, GOSAT-GW in summer 2025. NASA successfully launched the Orbiting Carbon Observatory-2 (OCO-2) in 2014 (Crisp et al., 2017). These are polar, low earth orbiting satellites that collect observations at a given location every 3–16 days at the same local time, usually near local noon. In 2019, NASA installed OCO-3 aboard the International Space Station (ISS; Taylor et al., 2020). OCO-3 is nearly the same instrument as OCO-2, but the ISS follows a complicated orbit that enables observations at different times of the day (Taylor et al., 2023).

X_{CO2} is also measured by ground-based networks, including the Total Carbon Column Observing Network (TCCON). TCCON consists of upward looking Fourier Transform Spectrometers (FTSs) that use direct solar absorption spectrometry to measure X_{CO2} and the total column abundance of other greenhouse gases (Wunch et al., 2010). The network provides observations of diurnally varying X_{CO2}, since up to a few hundred spectra per day can be measured during sunlit conditions. Keppel-Aleks et al. (2012) and Torres et al. (2019) showed that climatological diurnal drawdown in X_{CO2} observed at the TCCON site in Park Falls, Wisconsin (46°N, 90°W) agreed well with collocated eddy covariance fluxes, which are estimated from coincident observations of high-frequency (10 Hz) observations of boundary layer CO_2 and 3-dimensional turbulent winds (Baldocchi, 2003). In these studies, all days with sufficient observations to infer diurnal drawdown were averaged within a calendar month. The diurnal drawdown was typically small, at most 1–1.5 ppm decreases from morning to afternoon during the peak of the growing season, consistent with estimates derived from running terrestrial ecosystem model fluxes through an atmospheric transport model (Keppel-Aleks et al., 2011).

Notably, Keppel-Aleks et al. (2012) showed that the agreement with eddy covariance drawdown was poor when individual days were compared. They attributed this mismatch to mesoscale and synoptic scale atmospheric transport modifying the CO_2 mole fraction on timescales of a few hours. Such atmospheric transport would manifest as a change in X_{CO2} without affecting the eddy covariance flux estimate. The northern hemisphere extratropical atmospheric X_{CO2} gradient is maximized during the summer growing season (Olsen & Randerson, 2004), and advection of X_{CO2} via large-scale eddies in the form of synoptic scale weather systems can contribute greater within-day variability of X_{CO2} than the variation expected due to local ecosystem fluxes (Torres et al., 2019). Furthermore, smaller scale mesoscale transport causes variations by as much as half of the diurnal change of X_{CO2} (Mitchell et al., 2023; Torres et al., 2019).

In this manuscript we first provide an assessment of the capacity of OCO-3 to directly infer the climatological diurnal cycle of X_{CO2}. We then determine the minimum number of space-based observations required to quantify the diurnal cycle of X_{CO2} using a combination of ground-based X_{CO2} data from TCCON and simulated X_{CO2} within a bootstrapping approach. Section 2 introduces the data sets and methods for identifying the minimum number of required observations to estimate the diurnal cycle of X_{CO2}. We present results in Section 3 and discuss the implications for X_{CO2} observing strategies in Section 4.

2. Data and Methods

2.1. OCO-3

The OCO-3 instrument measures X_{CO2} aboard the International Space Station (ISS), whose orbital period is around ∼92 min, with a 3-day repeat cycle albeit at a different time in the diurnal cycle due to the precessing orbit (i.e., the equator crossing time is early by 20 min each day). The orbital inclination of the ISS is 51.6°, which limits latitudinal data coverage to within roughly 52° of the equator in each hemisphere. OCO-3 science observations began in August 2019 and were paused in October 2023. At that point, the instrument was temporarily

21698996, 2026, 1, Downloaded from https://agupubs.onlinelibrary.wiley.com/doi/10.1029/2025JD044301 by Spanish Cochrane National Provision (Ministerio de Sanidad), Wiley Online Library on [03/02/2026]. See the Terms and Conditions (https://onlinelibrary.wiley.com/terms-and-conditions) on Wiley Online Library for rules of use; OA articles are governed by the applicable Creative Commons License

Table 1
TCCON Sites and Dates of Measurements Used in This Analysis

TCCON site	Acronym	Location	Citation	Dates of TCCON measurements
Park Falls, WI, US	pa	45.93°N, 90.44°W	Wennberg et al. (2022)	26 May 2004–12 December 2022
Lamont, OK, US	oc	36.69°N, 97.56°W	Wennberg et al. (2025)	6 July 2008–12 December 2022
Izana, Tenerife	iz	28.31°N, 16.50°W	García et al. (2022)	7 January 2014–31 October 2022
Reunion Island	ra	20.90°S, 55.48°E	De Mazière et al. (2022)	1 March 2015–18 July 2020

removed from its port on the Japanese Experimental Module, but observations resumed in 2024. Unlike OCO-2, which has a consistent 16-day repeat cycle globally (Crisp et al., 2004), the OCO-3 repeat cycle is more complex, with an average repeat cycle of approximately 70 days for OCO-3 to observe the same location at the same time of day (Eldering et al., 2019).

The OCO-3 instrument is described in depth in Eldering et al. (2019) and Taylor et al. (2020) but a brief description is provided here. OCO-3 consists of three grating spectrometers, measuring reflected sunlight in a strong CO_2 absorption band centered around 2.0 μm, a weak CO_2 absorption band near 1.6 μm, and the oxygen A band near 0.76 μm. Each measurement consists of eight cross-track footprints of 1.6 by 2.2 km^2, obtained over 0.33 s. Unlike OCO-2, the spectrometers on OCO-3 are guided by a pointing mirror assembly (PMA), which allows for measurements of irradiances at various solar zenith angles. Observations are made with OCO-3 in several scanning modes: land nadir, land and ocean glint, target mode, and Snapshot Area Mapping (SAMs) (Eldering et al., 2019), and we use all available modes in this analysis.

In this study, we use the V11r Level 2 bias-corrected X_{CO2} from the full-physics retrieval product (OCO3_L2_Lite_FP 11; O'Dell et al., 2018), incorporating observations from August 2019 through 30 June 2025, with a pause from 12 November 2023 through 16 July 2024. X_{CO2} is retrieved from the measured irradiances, combined with ancillary meteorological and spectroscopic data, using the Atmospheric Carbon Observations from Space (ACOS) retrieval algorithm (O'Dell et al., 2018; Taylor et al., 2023). For OCO-3, X_{CO2} retrievals are accurate to within 1 ppm after calibration with the TCCON network (Eldering et al., 2019; Taylor et al., 2023). Based on analysis of OCO-2 observations which use the same retrieval algorithm, precision is generally better than 0.5 ppm (Mitchell et al., 2023). We use output from the quality control parameter in the OCO3_L2_Lite_FP 11output to retain observations whose quality flag is set to zero.

2.2. TCCON

TCCON is a global, ground-based network of Fourier transform spectrometers (FTS) that measure direct solar absorption spectra in the near-infrared, from which the total column-averaged mole fraction of atmospheric trace gasses including CO_2, methane (CH_4), nitrous oxide (N_2O), carbon monoxide (CO), water vapor (H_2O) and semi-heavy water (HDO) are inferred (Wunch, Toon, et al., 2011). TCCON is regularly used for validating OCO-2 and -3 X_{CO2} retrievals (Das et al., 2025; Taylor et al., 2023; Wunch et al., 2011b, 2017) and provides a long-term record with dense temporal coverage. In the absence of all cloud cover, a spectrum can be obtained approximately every 2 min. Retrievals of X_{CO2} are derived from absorption in the 1.58 and 1.60-μm absorption band (Wunch, Toon, et al., 2011) that are consistent with OCO-3's weak CO_2 band. TCCON data have been calibrated to the World Meteorological Organization (WMO) CO_2 scale using periodic aircraft and AirCore overpasses (Karion et al., 2010; Wunch et al., 2010) and typically have precision better than 0.4 ppm.

We calculate the climatological diurnal cycle in X_{CO2} using observations from four TCCON sites: two mid-latitude sites in the interior of North America, and two island sites (one subtropical and one tropical; Table 1). We choose three different latitude zones because we expect that patterns of atmospheric transport, which vary by latitude, may differentially impact our ability to estimate the diurnal cycle (Torres et al., 2019). In addition to atmospheric transport, the seasonality of local fluxes varies by latitude (Torres et al., 2019), and the regional impact will vary for continental versus island sites. To compare TCCON with OCO-3, we follow the coincident criteria described by Wunch et al. (2017) in which any retrieval within a 10° longitude and 5° latitude centered over a TCCON location is considered coincident, using all available viewing modes (Figure 1). We partition all available data within hourly bins for each OCO-3 overpass. We use TCCON data that has been processed using the GGG2020 retrieval algorithm (Laughner et al., 2024), filtering out any data where the solar zenith angle is

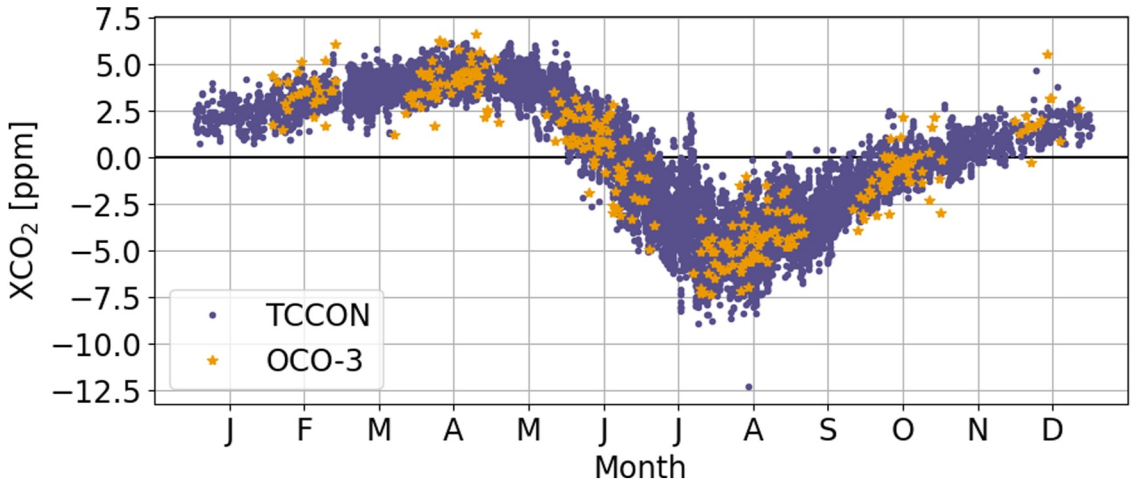

Figure 1. Annual cycle of X_{CO2} detrended anomalies at Park Falls, WI. TCCON data (purple) have been detrended, with multiple years overlaid. The spread on any given day arises from interannual variability, synoptic variability, and diurnal fluxes. OCO-3 X_{CO2} data (orange) coincident with Park Falls between 2019 and 2025 are overlain on the TCCON data.

greater than 70° since airmass-dependent biases are more likely in spectra obtained at high solar zenith angle (Laughner et al., 2024).

2.3. CarbonTracker

We use CO_2 output from the CarbonTracker data assimilation system (Peters et al., 2007) to corroborate inferences about the detectability of the diurnal cycle made from TCCON. CarbonTracker simulates 4-dimensional atmospheric CO_2 fields (x, y, z, and t) by assimilating in situ CO_2 observations via the TM5 atmospheric transport model (Krol et al., 2005) bounded by meteorological data from the European Center for Medium-Range Weather Forecasts (ECMWF) ERA-interim reanalysis product (Dee et al., 2011). In this study, we use the CO_2 and temperature products provided by the 2022 version of CarbonTracker (CT2022; Jacobson et al., 2023). The temporal resolution of CT2022 output is every 3 hr, from January 2000 to the end of February 2021. The CT2022 horizontal resolution over our study region in North America rests on 1° by 1° grid cells and 3° by 2° grid cells in the rest of the world (Jacobson et al., 2023). Because the non-North American sites we focus on in this paper are on small islands, CT2022 does not estimate sufficiently large grid cell level fluxes to quantify a meaningful diurnal cycle; our focus is therefore on Park Falls and Lamont when comparing to CT2022. For these sites, we integrate CO_2 vertically for the nearest horizontal grid cell to compute X_{CO2}.

2.4. NCEP Reanalysis

We develop a synoptic correction for X_{CO2} using 700 hPa potential temperature extracted from National Centers for Environmental Prediction–Department of Energy (NCEP–DOE) Atmospheric Model Intercomparison Project (AMIP-II) reanalysis output (henceforth described as NCEP reanalysis). NCEP reanalysis is a physically based atmospheric model constrained by a 3-dimensional variational (3D-Var) data assimilation scheme (Kanamitsu et al., 2002). NCEP Reanalysis operates as a global spectral model evaluated over 28 sigma vertical levels and a T62 Gaussian grid, which translates to a horizontal grid resolution of approximately 210 by 210 km. The temporal resolution of the model is 6 hr, and reanalysis output is available from January 1979 through March 2025.

2.5. Estimating the Climatological Diurnal Cycle of XCO_2

We isolate the diurnal signal in X_{CO2} using the same method as Torres et al. (2019). First, we average the timeseries into daily mean values and fit a second order polynomial to the timeseries. After subtracting the trend, we calculate the climatological seasonal cycle as the monthly mean of the detrended data. For each site we analyze, each calendar month has between 42 and 337 days where observations were obtained across the multi-year record, since data collection can only occur under clear-sky conditions. We note that TCCON observations can only be obtained under clear sky, daylight conditions, but previous analysis has suggested the imprint of this

21698996, 2026, 1, Downloaded from https://agupubs.onlinelibrary.wiley.com/doi/10.1029/2025JD044301 by Spanish Cochrane National Provision (Ministerio de Sanidad), Wiley Online Library on [03/02/2026]. See the Terms and Conditions (https://onlinelibrary.wiley.com/terms-and-conditions) on Wiley Online Library for rules of use; OA articles are governed by the applicable Creative Commons License

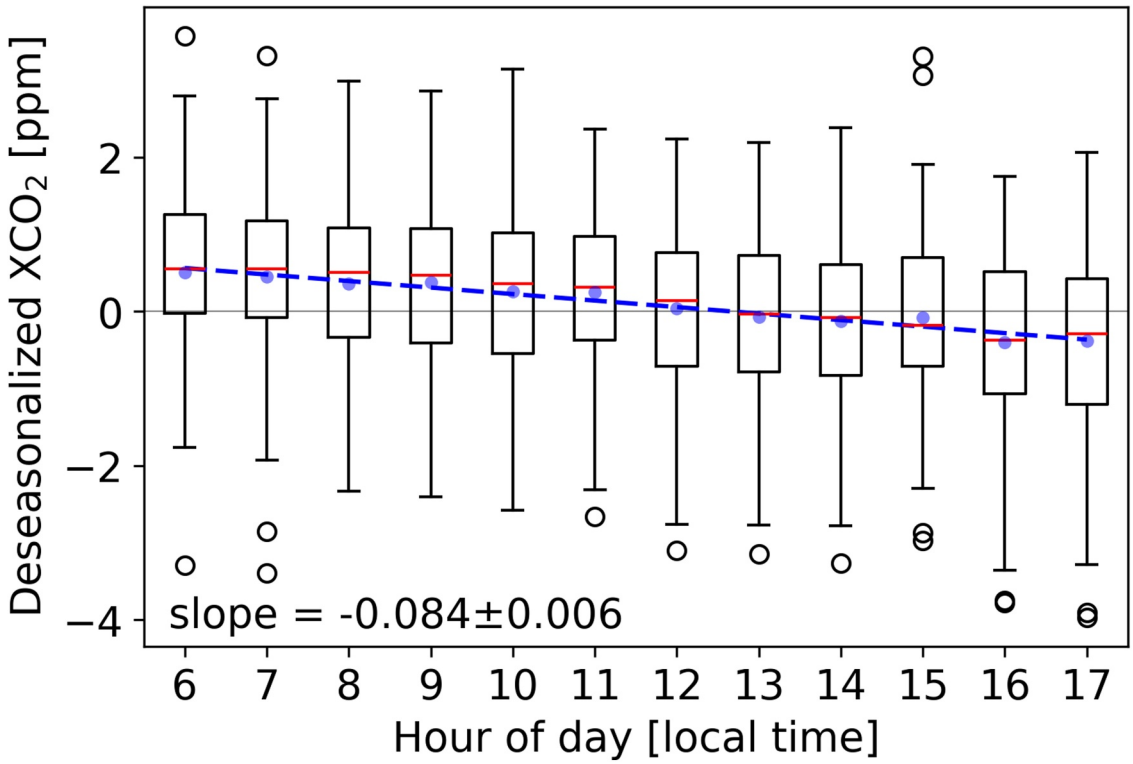

Figure 2. Example of diurnal cycle calculation for the month of June at Park Falls. Individual detrended and deseasonalized observations are binned by hour. Red lines represent the hourly median and blue dots are the hourly mean value. Boxes extend from the first quartile (Q1) to the third quartile (Q3) and whiskers extend to the farthest data point lying within 1.5x the interquartile (Q3–Q1) range from the box. Data outside this range are shown as open circles. For each calendar month, the hourly rate of change (dashed blue line) is fit through all hours with solar zenith angle SZA < 70°. In this example, the slope was 0.084 ppm hr^{-1}, with 12 daylight hours, leading to a diurnal change of −1.01 ± 0.07 ppm.

sampling bias is small (Keppel-Aleks et al., 2012). The trend and climatological seasonal cycle are then subtracted from all X_{CO2} soundings. For TCCON and CT2022, where there are sufficiently long records of data, we detrend and deseasonalize using X_{CO2} data from their respective data sets. Given the limited data available for OCO-3, we detrend and deseasonalize OCO-3 X_{CO2} data using values derived from the coincident TCCON site. The resulting detrended and deseasonalized timeseries contains the imprint of interannual variability, transport-driven variability, and the diurnal variability we seek to quantify.

We calculate the climatological diurnal cycle for monthly timescales at each site using detrended and deseasonalized X_{CO2} data from TCCON. For each calendar month, we partition observations into hourly bins. We take the mean of all the data in each bin for which there are at least 3 observations, filtering out data obtained at solar zenith angles greater than 70° (Figure 2) The diurnal change is then determined by fitting a slope through the hourly bins [ppm/hour] and multiplying by the number of hours for which SZA < 70°, to get a value with units [ppm]. We note that this diurnal change represents only the diurnal change during daylight hours, and thus the magnitude in part scales with the number of daylight hours with SZA < 70° for a given month. In months where the within-day X_{CO2} change is non-monotonic, this method may underestimate the diurnal amplitude. However, this calculation yields similar estimates (within 0.2 ppm) as calculating the diurnal amplitude from the maximum and minimum values, when averaged for all days within a calendar month, and has smaller uncertainty (Figure S1 in Supporting Information S1). We note that our approach assumes that the influence of mesoscale and synoptic scale transport averages out. Throughout the rest of the observational analysis, we treat the monthly estimates of the climatological diurnal cycle derived from TCCON data as the "true" diurnal cycle of X_{CO2}, based on favorable comparisons with diurnally integrated eddy covariance fluxes shown in Keppel-Aleks et al. (2012) and Torres et al. (2019).

21698996, 2026, 1, Downloaded from https://agupubs.onlinelibrary.wiley.com/doi/10.1029/2025JD044301 by Spanish Cochrane National Provision (Ministerio de Sanidad), Wiley Online Library on [03/03/2026]. See the Terms and Conditions (https://onlinelibrary.wiley.com/terms-and-conditions) on Wiley Online Library for rules of use; OA articles are governed by the applicable Creative Commons License

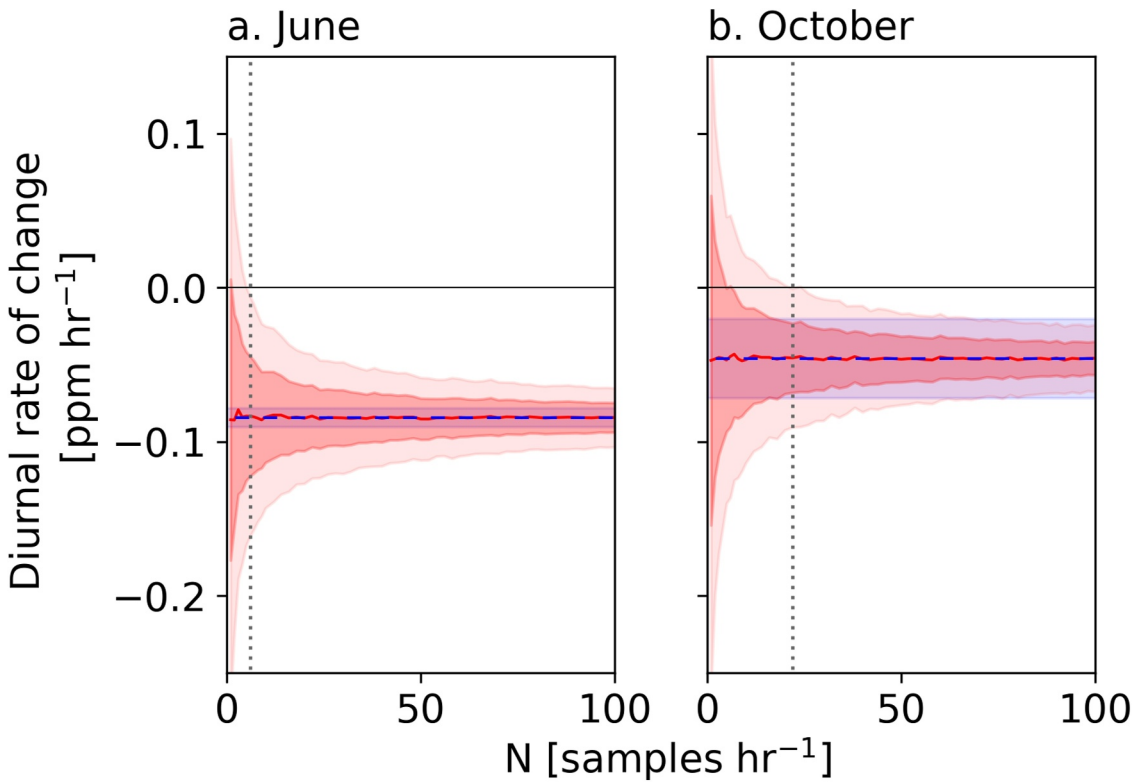

Figure 3. Bootstrapped diurnal drawdown at Park Falls for two representative months. The true slope fit from all TCCON data is shown by the blue dashed line. The mean slope fit from 1,000 bootstrap realizations is shown by the red curve, which varies as a function of N. The standard deviation on the slope fit across the 1,000 realizations is given by the red shading, with one and two standard deviations shown. The N at which the diurnal slope is detectable is found where the 2-sigma uncertainty on the bootstrapped slope excludes zero (dotted vertical line). For June, this occurs at $N_{required} = 6$ whereas for October, this occurs at $N_{required} = 22$.

2.6. Bootstrapping the Diurnal Cycle of XCO_2

We use a bootstrapping approach to determine how many data points are required in each hour bin to robustly calculate the diurnal cycle. We partition all the detrended and deseasonalized TCCON X_{CO2} data into hourly bins as described in Section 2.2. We then sample with replacement across all hourly bins to create 1,000 realizations of the diurnal cycle, in which each realization contains N observations per hour. We vary N between 1 and 100. For each of the 1,000 realizations for a given N, we fit a slope through the hour bin mean values to determine the diurnal rate of change. We then calculate, as a function of N, the mean and standard deviation of the diurnal rate of change across the 1,000 realizations. We calculate $N_{required}$ as the minimum value of N where the diurnal rate of change is considered observable for a given N, defined as when the 2-sigma confidence interval excludes zero (e.g., Figure 3). We follow the same procedure for CT2022 data, using model output at 3-hr intervals. Although detectability is based on the 2-sigma range of the bootstrapped diurnal rate of change excluding zero, we report diurnal change values in units [ppm], where the rate of change is multiplied by the number of hours where the SZA is less than 70°.

2.7. Accounting for Synoptic Variations

We conducted a sensitivity test to determine whether an empirical correction to account for synoptic scale advection reduced the $N_{required}$ to robustly detect a diurnal change (Figure 4). Keppel-Aleks et al. (2012) showed that at mid-latitude TCCON sites, the daily mean X_{CO2} value could change by up to a few ppm from 1 day to the next due to synoptic advection. Such variations are correlated with variations in potential temperature at 700 hPa (Θ_{700}), a dynamical tracer of effective latitude. At each site, we therefore apply a 3–21 days bandpass filter, selected for consistency with previous analysis by Keppel-Aleks et al. (2011); Keppel-Aleks et al. (2012), to both the observed X_{CO2} from TCCON and 700 hPa potential temperature from the coincident NCEP reanalysis data. We fit a linear slope to the bandpass filtered variables (Figure 4b) for each calendar month (Figure 4a). The

21698996, 2026, 1, Downloaded from https://agupubs.onlinelibrary.wiley.com/doi/10.1029/2025JD044301 by Spanish Cochrane National Provision (Ministerio de Sanidad), Wiley Online Library on [03/03/2026]. See the Terms and Conditions (https://onlinelibrary.wiley.com/terms-and-conditions) on Wiley Online Library for rules of use; OA articles are governed by the applicable Creative Commons License

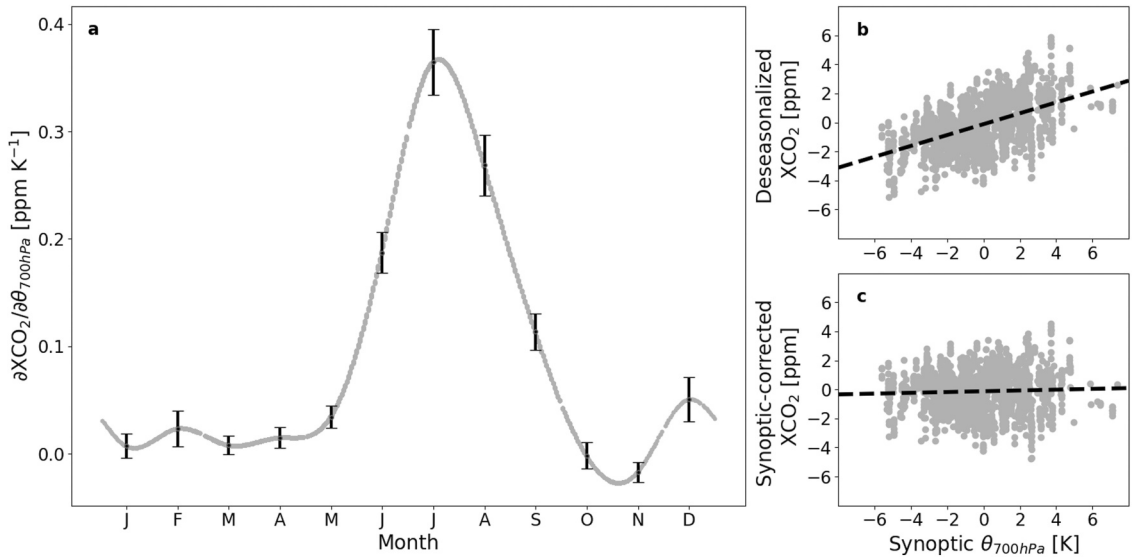

Figure 4. Methodology for synoptic correction. (a) Shows the relationship between fluctuations in X_{CO2} and potential temperature at 700 hPa (Θ_{700}), calculated for each month (black symbols). A cubic spline is fit to the 12 monthly values to derive a daily mean value. (b) Shows the raw relationships between deseasonalized X_{CO2} and Θ_{700} used in panel a for the month of July. (c) Shows the relationship between synoptic-corrected X_{CO2} and deseasonalized Θ_{700} after removing the day-of-year specific slope from panel (a).

calculated slopes vary seasonally, and are largest during the Northern Hemisphere growing season when north–south gradients in X_{CO2} are largest (Figure 4a; Keppel-Aleks et al., 2011) and are at a minimum during the winter when meridional gradients are small. We then fit a cubic spline to the monthly means to estimate a day-of-year relationship between X_{CO2} and potential temperature (gray line in Figure 4a). For any given day, we multiply the reanalysis deseasonalized Θ_{700} value by the day-of-year slope and subtract this value from the observed X_{CO2} (Figure 4c).

3. Results

TCCON data, after detrending and deseasonalizing, show a clear diurnal cycle. At the Park Falls TCCON site (Washenfelder et al., 2006), observations made during the growing season (May–September) show morning observations that are above the annual mean, whereas late afternoon observations are below the annual mean, indicating net ecosystem carbon drawdown over the course of the day (Figure 5). From morning to afternoon, the overall daylight amplitude is at most 1 ppm, indicating that local fluxes impart a small drawdown. This value is consistent with estimates from integrated eddy covariance observations (Keppel-Aleks et al., 2012) and simulations of the diurnal cycle in the column (Keppel-Aleks et al., 2011). Most hour-month bins, with the exception of those at the beginning or end of the day, comprises at least 100 observations (Figure 5; Figures S2–S4 in Supporting Information S1), so random noise in the observations as well as the impact of within-day transport phenomena are most likely averaged out. In contrast, the OCO-3 data show no consistent diurnal patterns. Hourly anomalies can be as large as 2 ppm, which may be due to the low number of observations in any hour-month bin. At most—14 OCO-3 observations have been collected at the Park Falls TCCON site in any given hour-month bin, and many bins either lack observations or have less than 5 observations. The large hourly anomalies might therefore reflect large random noise in the OCO-3 observations or the fact that X_{CO2} can vary on any given day due to synoptic activity in the atmosphere (Keppel-Aleks et al., 2012).

The number of observations required to exclude a diurnal rate of change of zero varies as a function of month. For the Park Falls TCCON site, diurnal changes range from morning-to-afternoon increases of 0.3 ppm outside the growing season to 1 ppm drawdown during the growing season (Figure 6). Diurnal changes are negative between May and October. During the growing season when the diurnal change is relatively large, between 7 and 30 observations per daylight hour are required to exclude a diurnal change of 0. Outside the growing season, the diurnal signal is smaller and between 25 and 60 observations per daylight hour are required to infer non-zero diurnal changes. We note that there are 3 months where the slope could not robustly exclude zero (April,

21698996, 2026, 1, Downloaded from https://agupubs.onlinelibrary.wiley.com/doi/10.1029/2025JD044301 by Spanish Cochrane National Provision (Ministerio de Sanidad), Wiley Online Library on [03/03/2026]. See the Terms and Conditions (https://onlinelibrary.wiley.com/terms-and-conditions) on Wiley Online Library for rules of use; OA articles are governed by the applicable Creative Commons License

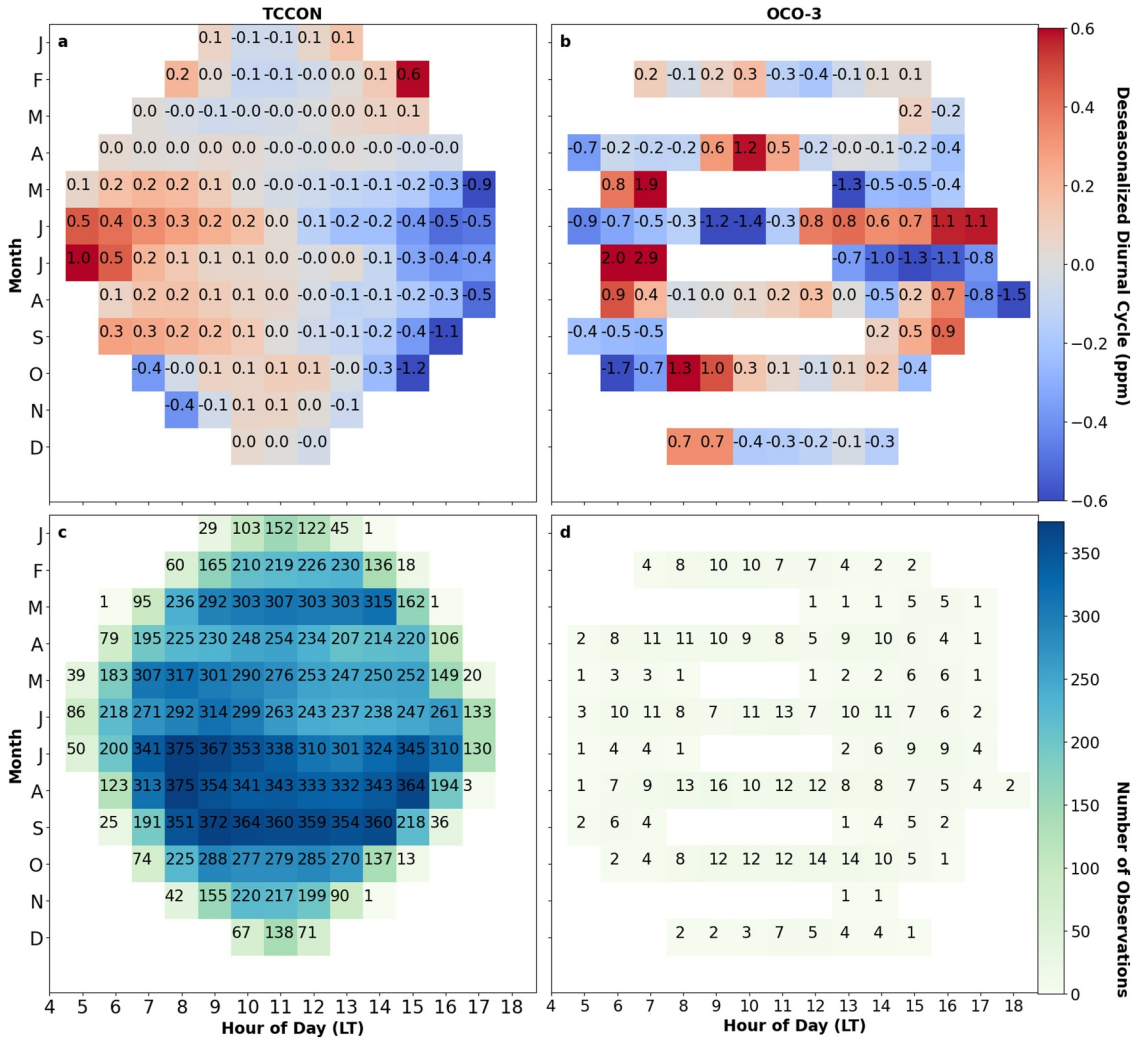

Figure 5. The diurnal signal in X_{CO2} for the Park Falls (a) TCCON and (b) spatially co-located OCO-3, calculated by detrending and deseasonalizing raw data, then calculating the hourly mean for all X_{CO2} acquired within the specified hourly bin shown in local time (LT). For TCCON, panel (c) shows that the hourly bins contain at least 100 X_{CO2} soundings, but for OCO-3 (d), the number of observations is typically less than 10.

November, and December). In April, the true diurnal rate of change is close to zero so this result is expected. Due to low sun angles during winter, a slope cannot be calculated in December because only 1 hr bin has SZA less than 70°. The fact that the sunlit portion of the day is longer during summer than winter increases the diurnal change magnitude, since the number of daylight hours is longer, and also improves detectability. In a sensitivity test where the diurnal rate of change was fit to a truncated hourly range (the hours available for the spring equinox in March), the slopes for summer months were slightly smaller than those fit using all available daylight hours (Figure S5a in Supporting Information S1). Given the nonlinearity of the detectability curves shown in Figure 3, the smaller diurnal rate of changes inferred from truncated days led to increased values of $N_{required}$ (Figure S5c in Supporting Information S1).

Similar patterns are seen at the other three TCCON locations we analyze (Figure S6 in Supporting Information S1). At Lamont, the diurnal change is zero or negative throughout the year, with the largest diurnal changes of −0.8 to 0.9 ppm (negative sign indicating ecosystem drawdown) during mid-summer. The growing season is broader than at Park Falls (March–October in Figure S6a of Supporting Information S1 compared to May–September in Figure 6a), which may be due to the impacts of crops with distinct phenological cycles, including winter wheat (Riley et al., 2009; Wagle et al., 2019). Izana, a subtropical island site, has smaller diurnal changes (<0.3 ppm) with negligible seasonality (Figure S6b in Supporting Information S1). At Reunion Island, a tropical island site, diurnal

21698996, 2026, 1, Downloaded from https://agupubs.onlinelibrary.wiley.com/doi/10.1029/2025JD044301 by Spanish Cochrane National Provision (Ministerio de Sanidad), Wiley Online Library on [03/03/2026]. See the Terms and Conditions (https://onlinelibrary.wiley.com/terms-and-conditions) on Wiley Online Library for rules of use; OA articles are governed by the applicable Creative Commons License

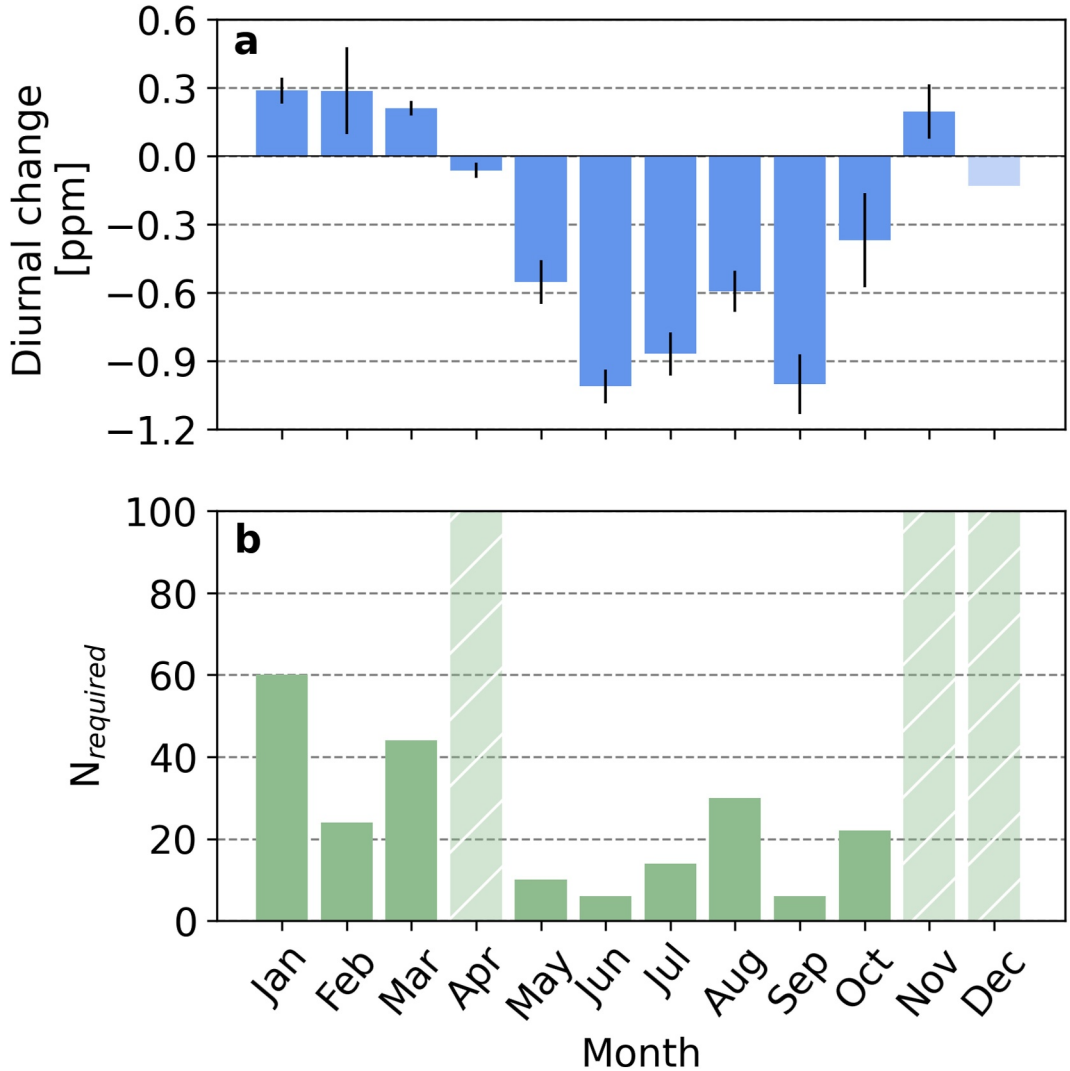

Figure 6. (a) Diurnal changes in X_{CO2} calculated from the Park Falls TCCON across all calendar months and (b) the corresponding number of observations per hour required to detect a diurnal rate of change that excludes 0 ppm hr^{-1} within two standard deviations of the mean. Months in which a robust diurnal signal cannot be calculated with 100 observations per hour are shown in hatched bars.

changes are as large as 0.9 ppm, but most months have changes between 0.2 and 0.6 ppm. It is noteworthy that the two island sites have smaller diurnal changes than the two continental sites, which may be due to integrated diurnal uptake within the field of influence of the TCCON instrument being greater at Park Falls and Lamont. All months with robust diurnal changes show net uptake, consistent with warm temperatures and adequate moisture. Across all four sites, $N_{required}$ decreases nonlinearly as the observed diurnal change increases (Figure 7; Figure S6 in Supporting Information S1). Diurnal changes larger than 0.5 ppm tend to have $N_{required}$ values between 5 and 30, whereas for diurnal changes smaller than 0.5 ppm, $N_{required}$ increases hyperbolically.

Analysis of CT2022 posterior X_{CO2} fields corroborates results with TCCON observations. During the growing season, between 5 and 60 observations per hour are required to robustly quantify the slope (Figure 8) at Park Falls. The small drawdown values outside the growing season for CT2022 are likewise not detectable even with 100 observations per hour. These $N_{required}$ are slightly higher than those determined from the TCCON observations at Park Falls, but we note that the drawdown values are smaller in CT2022 (maximum values around 0.5 ppm during June and July, compared to values around 0.9 ppm for TCCON). The smaller magnitude is due in part to the fact that CT2022 data are output at 3-hr intervals rather than hourly. When we conducted a sensitivity test with

21698996, 2026, 1, Downloaded from https://agupubs.onlinelibrary.wiley.com/doi/10.1029/2025JD044301 by Spanish Cochrane National Provision (Ministerio de Sanidad), Wiley Online Library on [03/02/2026]. See the Terms and Conditions (https://onlinelibrary.wiley.com/terms-and-conditions) on Wiley Online Library for rules of use; OA articles are governed by the applicable Creative Commons License

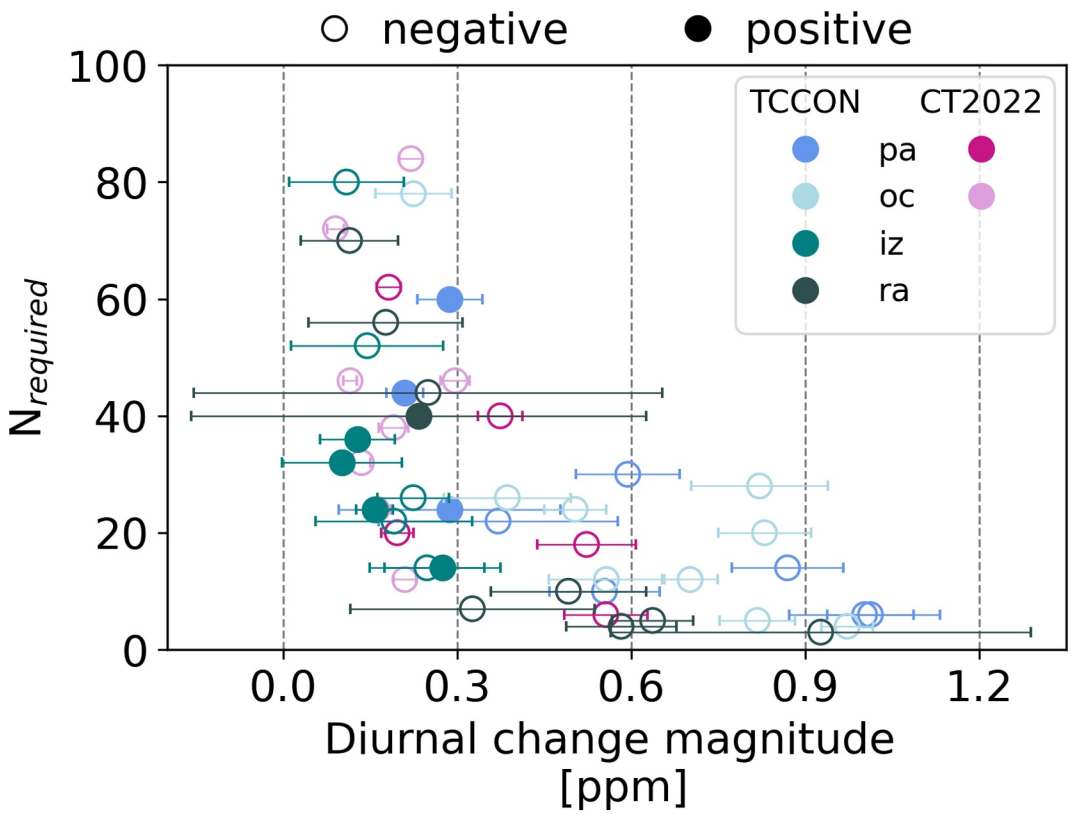

Figure 7. Summary of $N_{required}$ across TCCON sites for the diurnal rate of change, plotted as a function of the calculated monthly diurnal change. Observations are plotted in cool colors, and CT2022 data are plotted in warm colors. Site acronyms are provided in Table 1.

TCCON data aggregated to 3 hrs, the resulting diurnal change magnitudes were around 0.1–0.3 ppm smaller (Figure S7 in Supporting Information S1 compared to Figure 6 and Figure S6 in Supporting Information S1). We note, however, that the diurnal cycle in CT2022 is not optimized against diurnal observations during the inversion itself, thus we do not expect the diurnal cycle in CT2022 XCO_2 to match that in TCCON at the same sites. Given the smaller diurnal cycle in CT2022 compared to TCCON, the higher $N_{required}$ for CT2022 is consistent with those derived from TCCON (Figure 7).

The use of the synoptic correction does not provide a robust reduction in $N_{required}$ across sites or months of the year. At Park Falls, June–August show a reduction in $N_{required}$ of around 5 (Figure 9). We note that this time of the year is when synoptic variations are largest in the midlatitudes. However, outside the growing season, the synoptic correction either makes little difference, or increases the number of observations required (e.g., March). At the other sites, the synoptic correction tends overall to increase the number of observations required (Figure S8 in Supporting Information S1).

4. Discussion and Conclusions

Our results show that, to date, OCO-3 has not collected enough data for any of the four TCCON sites we analyzed to make direct inferences of the climatological diurnal cycle of XCO_2 (Figures 5 and 6, and Figures S2–S4 in Supporting Information S1). The result is consistent across sites that span a range of latitudes, ecosystem types, and continental and island geographies, which suggests that our conclusion would remain broadly unchanged if other locations were analyzed. However, we leverage the longevity of coincident temporally dense TCCON observations at each site to calculate a climatological diurnal cycle of XCO_2 (e.g., Figure 1 for Park Falls). The climatological diurnal changes at all four TCCON sites are small (<1 ppm), with the largest diurnal changes occurring during the local growing season and at the continental sites.

21698996, 2026, 1, Downloaded from https://agupubs.onlinelibrary.wiley.com/doi/10.1029/2025JD044301 by Spanish Cochrane National Provision (Ministerio de Sanidad), Wiley Online Library on [03/03/2026]. See the Terms and Conditions (https://onlinelibrary.wiley.com/terms-and-conditions) on Wiley Online Library for rules of use; OA articles are governed by the applicable Creative Commons License

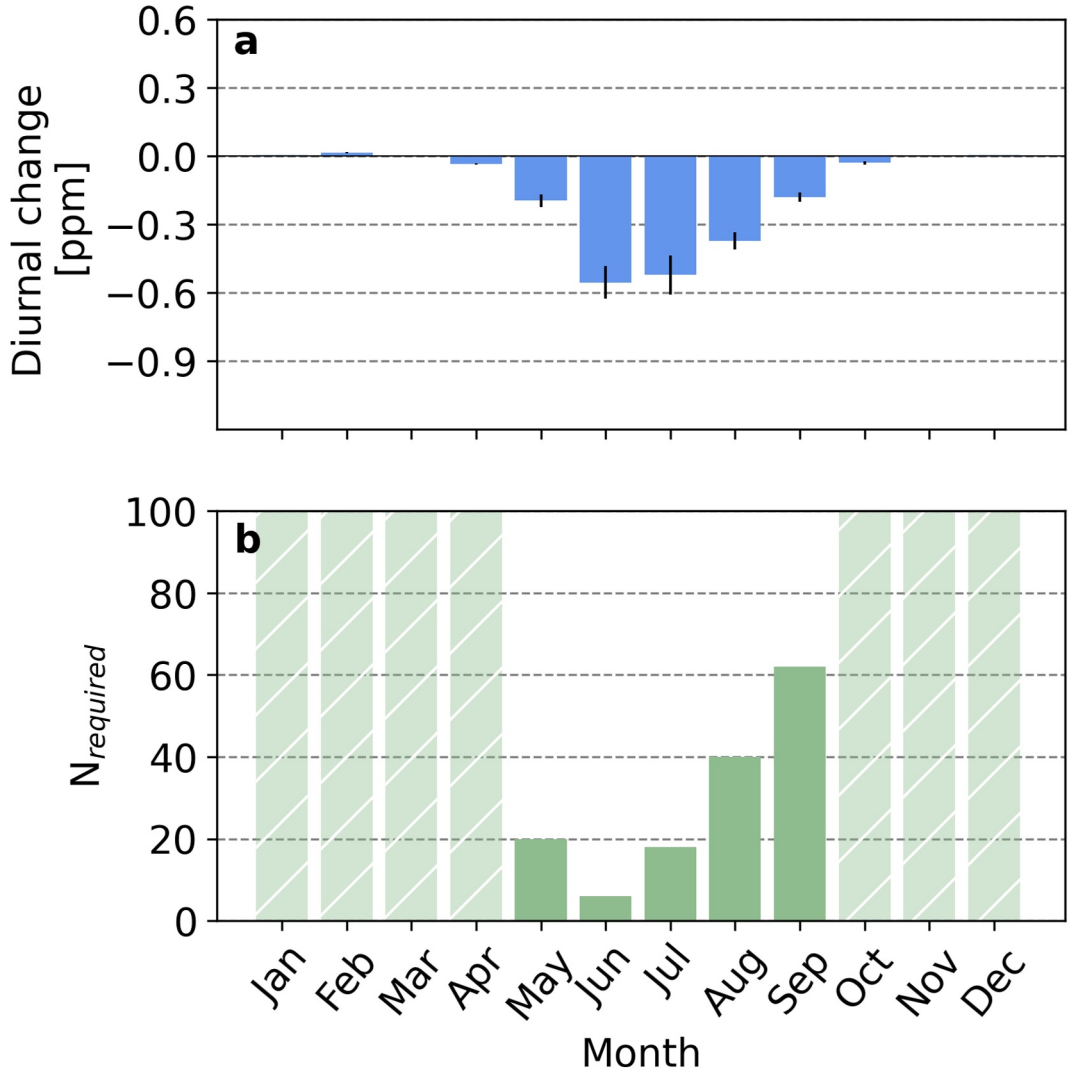

Figure 8. Same as Figure 6, except using CarbonTracker X_{CO2} instead of TCCON X_{CO2} at the Park Falls site.

Our analysis consistently shows that there must be of order 10 observations each daylight hour to robustly detect the diurnal change on monthly timescales. It is noteworthy that this result was consistent across each site using TCCON, and Park Falls and Lamont with CT2022 data. In general, the number of observations required scales with the magnitude of ecosystem drawdown, with generally fewer observations required when the diurnal drawdown is large (Figure 7). Our result that current observations from OCO-3 are insufficient to detect the diurnal cycle is consistent with Marchetti et al. (2025) who showed that when OCO-2 and OCO-3 sampled the same location within the same day, diurnal XCO_2 patterns could not be reliably inferred.

The correction for synoptic-scale variability based on a tracer of effective latitude did not meaningfully reduce $N_{required}$ across the sites and seasons we analyzed. Although this correction reduced $N_{required}$ at Park Falls during the peak of the growing season, when the Northern Hemisphere meridional gradient in X_{CO2} is largest, it generally increased $N_{required}$ at other sites and at other times of the year. This suggests that mesoscale variations, which impart variations of order 100 km or at timescales of hours and would not be expected to correlate with Θ_{700}, may be more important in masking the diurnal cycle in X_{CO2} than are larger, slower moving synoptic systems.

Even when accounting for atmospheric transport, other factors can impart variability in X_{CO2}, including retrieval errors in TCCON or OCO-3 or fossil fuel emissions. Even in the absence of retrieval errors with CT2022, we note a consistency in results when compared to TCCON data suggesting that TCCON retrieval error is not a major factor in determining $N_{required}$. Since OCO-3 has different error characteristics than TCCON, we expect that the $N_{required}$

21698996, 2026, 1, Downloaded from https://agupubs.onlinelibrary.wiley.com/doi/10.1029/2025JD044301 by Spanish Cochrane National Provision (Ministerio de Sanidad), Wiley Online Library on [03/02/2026]. See the Terms and Conditions (https://onlinelibrary.wiley.com/terms-and-conditions) on Wiley Online Library for rules of use; OA articles are governed by the applicable Creative Commons License

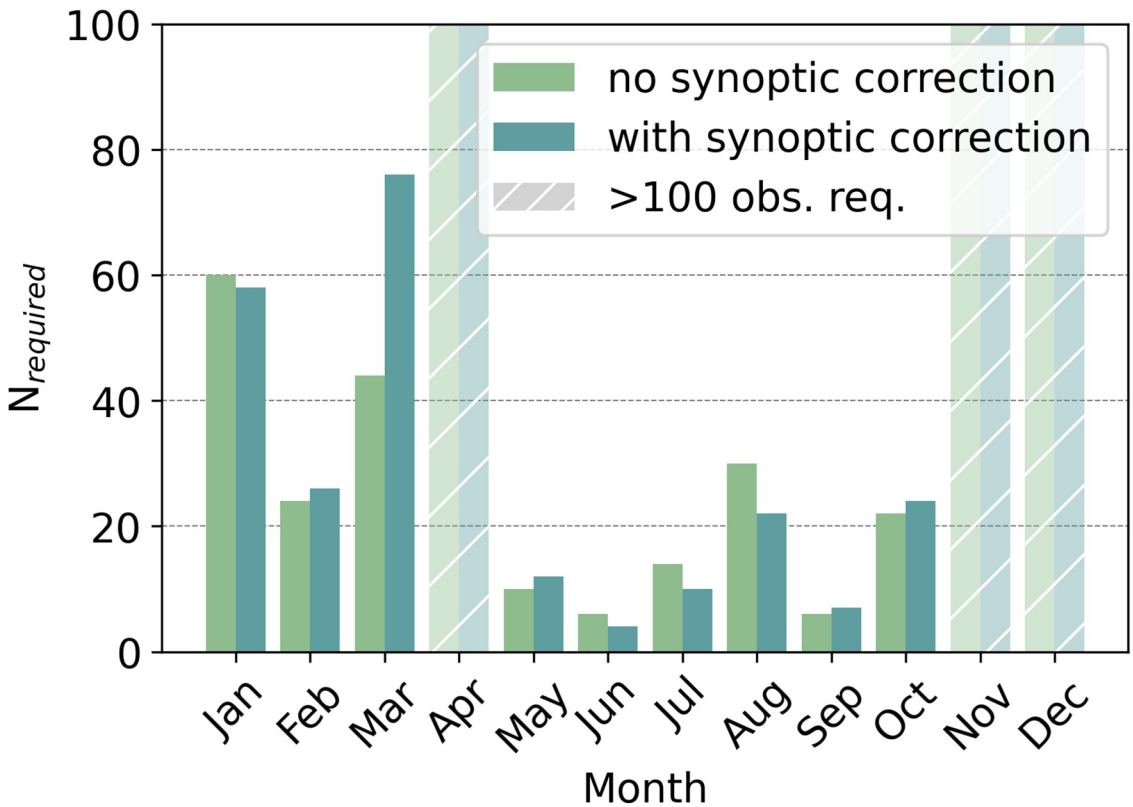

Figure 9. Differences between $N_{required}$ at Park Falls with and without the synoptic correction.

we report here may underestimate the number of OCO-3 soundings required to average away random noise in the space-based observation. Mitchell et al. (2023) reported random noise values up to 0.5 ppm for OCO-2 observations over North America; assuming similar error characteristics for OCO-3 at least 25 observations per hour would be required for the error on the hourly mean to be 0.1 ppm. Moreover, biases in the space-based retrieval may complicate robust observation of the diurnal cycle, since airmass dependent biases (Laughner et al., 2024) could differentially affect early morning or late afternoon observations, and factors such as viewing geometry, surface characteristics, and aerosol contribute additional bias to the OCO-3 observations (Bell et al., 2023).

Although additional years of data from OCO-3's extended mission will increase the number of overpasses at a specific location and may permit detection of climatological diurnal cycles from OCO-3, the most straightforward path for space-based observations of the diurnal cycle of X_{CO2} would be from a geostationary orbit (e.g., GeoCarb; Moore et al., 2018) or from a constellation of satellites that share a common instrument and have different local overpass times, such as the Copernicus CO2M mission under active development by ESA and partners (Meijer et al., 2023). Using OCO-3 data alone, better constraints on mesoscale sources of variations may provide the best path for reducing the $N_{required}$.

Conflict of Interest

The authors declare no conflicts of interest relevant to this study.

Data Availability Statement

All observations and model output used in this analysis are available on public data repositories. TCCON data are publicly available at https://tccondata.org/. OCO-3 data are publicly available at the GES DISC (https://disc.gsfc.nasa.gov/datasets?keywords=oco3). CT2022 data are publicly available at https://gml.noaa.gov/ccgg/carbontracker/. Analysis of these data forms the basis of both the main text and the supplement and was conducted using

21698996, 2026, 1, Downloaded from https://agupubs.onlinelibrary.wiley.com/doi/10.1029/2025JD044301 by Spanish Cochrane National Provision (Ministerio de Sanidad), Wiley Online Library on [03/03/2026]. See the Terms and Conditions (https://onlinelibrary.wiley.com/terms-and-conditions) on Wiley Online Library for rules of use; OA articles are governed by the applicable Creative Commons License

Python version 3.9.15 and 3.9.18. Figures in the main text and the supplement were generated using matplotlib version 3.9.2.

Acknowledgments
The authors acknowledge support from NASA's OCO-2 and OCO-3 Science Teams (NASA Awards 80NSSC18K0897, 80NSSC21K1071 to the University of Virginia and 80NSSC18K0900, 80NSSC21K1070 to the University of Michigan) and from a NASA FINESST award. We thank P. Wennberg and other TCCON data providers. We thank A. Jacobson and the National Oceanographic and Atmospheric Administration Earth System Research Laboratory in Boulder, CO for providing CarbonTracker CT2022 data, available online at http://carbontracker.noaa.gov. The TCCON Principal Investigators acknowledge funding from their national funding organizations. TCCON data were obtained from the archive at https://tccondata.org.

References

Baldocchi, D. D. (2003). Assessing the eddy covariance technique for evaluating carbon dioxide exchange rates of ecosystems: Past, present and future. *Global Change Biology*, *9*(4), 479–492. https://doi.org/10.1046/j.1365-2486.2003.00629.x

Bell, E., O'Dell, C. W., Taylor, T. E., Merrelli, A., Nelson, R. R., Kiel, M., et al. (2023). Exploring bias in the OCO-3 snapshot area mapping mode via geometry, surface, and aerosol effects. *Atmospheric Measurement Techniques*, *16*(1), 109–133. https://doi.org/10.5194/amt-16-109-2023

Braswell, B. H., Sacks, W. J., Linder, E., & Schimel, D. S. (2005). Estimating diurnal to annual ecosystem parameters by synthesis of a carbon flux model with eddy covariance net ecosystem exchange observations. *Global Change Biology*, *11*(2), 335–355. https://doi.org/10.1111/j.1365-2486.2005.00897.x

Byrne, B., Baker, D. F., Basu, S., Bertolacci, M., Bowman, K. W., Carroll, D., et al. (2023). National CO_2 budgets (2015–2020) inferred from atmospheric CO_2 observations in support of the global stocktake. *Essd*, *15*(2), 963–1004. https://doi.org/10.5194/essd-15-963-2023

Crisp, D., Atlas, R. M., Breon, F. M., Brown, L. R., Burrows, J. P., Ciais, P., et al. (2004). The Orbiting Carbon Observatory (OCO) mission. *Advances in Space Research*, *34*(4), 700–709. https://doi.org/10.1016/j.asr.2003.08.062

Crisp, D., Pollock, H. R., Rosenberg, R., Chapsky, L., Lee, R. A. M., Oyafuso, F. A., et al. (2017). The on-orbit performance of the Orbiting Carbon Observatory-2 (OCO-2) instrument and its radiometrically calibrated products. *Atmospheric Measurement Techniques*, *10*(1), 59–81. https://doi.org/10.5194/amt-10-59-2017

Das, S., Kiel, M., Laughner, J., Osterman, G., O'Dell, C. W., Taylor, T. E., et al. (2025). Comparisons of the v11.1 Orbiting Carbon Observatory-2 (OCO-2) X_{CO2} measurements with GGG2020 TCCON. *Earth and Space Science*, *12*(7), e2024EA003935. https://doi.org/10.1029/2024EA003935

Dee, D. P., Uppala, S. M., Simmons, A. J., Berrisford, P., Poli, P., Kobayashi, S., et al. (2011). The ERA-interim reanalysis: Configuration and performance of the data assimilation system. *Quarterly Journal of the Royal Meteorological Society*, *137*(656), 553–597. https://doi.org/10.1002/qj.828

De Mazière, M., Sha, M. K., Desmet, F., Hermans, C., Scolas, F., Kumps, N., et al. (2022). TCCON data from Réunion Island (RE), release GGG2020.R0 (version R0) [Dataset]. *CaltechDATA*. https://doi.org/10.14291/tccon.ggg2020.reunion01.R0

Denning, A. S., Fung, I. Y., & Randall, D. (1995). Latitudinal gradient of atmospheric CO_2 due to seasonal exchange with land biota. *Nature*, *376*(6537), 240–243. https://doi.org/10.1038/376240a0

Denning, A. S., Takahashi, T., & Friedlingstein, P. (1999). Can a strong atmospheric CO_2 rectifier effect be reconciled with a "reasonable" carbon budget? *Tellus B: Chemical and Physical Meteorology*, *51*(2), 249–253. https://doi.org/10.1034/j.1600-0889.1999.t01-1-00010.x

Eldering, A., Taylor, T. E., O'Dell, C. W., & Pavlick, R. (2019). The OCO-3 mission: Measurement objectives and expected performance based on 1 year of simulated data. *Amt*, *12*(4), 2341–2370. https://doi.org/10.5194/amt-12-2341-2019

García, O. E., Schneider, M., Herkommer, B., Gross, J., Hase, F., Blumenstock, T., & Sepúlveda, E. (2022). TCCON data from Izana (ES), release GGG2020.R1 (version R1) [Dataset]. *CaltechDATA*. https://doi.org/10.14291/tccon.ggg2020.izana01.R1

Gurney, K. R., Law, R. M., Denning, A. S., Rayner, P. J., Baker, D., Bousquet, P., et al. (2002). Towards robust regional estimates of CO_2 sources and sinks using atmospheric transport models. *Nature*, *415*(6872), 626–630. https://doi.org/10.1038/415626a

Isamu, R., Matsunaga, T., Nakajima, M., Yoshida, Y., Shiomi, K., Morino, I., et al. (2023). Greenhouse gases Observing SATellite 2 (GOSAT-2): Mission overview. *Progress in Earth and Planetary Science*, *10*(1), 33. https://doi.org/10.1186/s40645-023-00562-2

Jacobson, A. R., Schuldt, K. N., Tans, P., Andrews, A., Miller, J. B., Oda, T., et al. (2023). *CarbonTracker CT2022*. NOAA Global Monitoring Laboratory. https://doi.org/10.25925/Z1GJ-3254

Kanamitsu, M., Ebisuzaki, W., Woollen, J., Yang, S.-K., Hnilo, J. J., Fiorino, M., & Potter, G. L. (2002). NCEP–DOE AMIP-II reanalysis (R-2). *Bulletin of the American Meteorological Society*, *83*(11), 1631–1644. https://doi.org/10.1175/bams-83-11-1631

Karion, A., Sweeney, C., Tans, P., & Newberger, T. (2010). AirCore: An innovative atmospheric sampling system. *Journal of Atmospheric and Oceanic Technology*, *27*(11), 1839–1853. https://doi.org/10.1175/2010JTECHA1448.1

Keppel-Aleks, G., Wennberg, P. O., & Schneider, T. (2011). Sources of variations in total column carbon dioxide. *Atmospheric Chemistry and Physics*, *11*(8), 3581–3593. https://doi.org/10.5194/acp-11-3581-2011

Keppel-Aleks, G., Wennberg, P. O., Washenfelder, R. A., Wunch, D., Schneider, T., Toon, G. C., et al. (2012). The imprint of surface fluxes and transport on variations in total column carbon dioxide. *Biogeosciences*, *9*(3), 875–891. https://doi.org/10.5194/bg-9-875-2012

Krol, M., Houweling, S., Bregman, B., van den Broek, M., Segers, A., van Velthoven, P., et al. (2005). The two-way nested global chemistry-transport zoom model TM5: Algorithm and applications. *Atmospheric Chemistry and Physics*, *5*(2), 417–432. https://doi.org/10.5194/acp-5-417-2005

Laughner, J. L., Toon, G. C., Mendonca, J., Petri, C., Roche, S., Wunch, D., et al. (2024). The total carbon column observing Network's GGG2020 data version. *Earth System Science Data*, *16*(5), 2197–2260. https://doi.org/10.5194/essd-16-2197-2024

Law, R. M., Peters, W., Rödenbeck, C., Aulagnier, C., Baker, I., Bergmann, D. J., et al. (2008). TransCom model simulations of hourly atmospheric CO_2: Experimental overview and diurnal cycle results for 2002. *Global Biogeochemical Cycles*, *22*(3). https://doi.org/10.1029/2007GB003050

Liu, J., Bowman, K. W., Schimel, D. S., Parazoo, N. C., Jiang, Z., Lee, M., et al. (2017). Contrasting carbon cycle responses of the tropical continents to the 2015-2016 El Niño. *Science*, *358*(6360), eaam5690. https://doi.org/10.1126/science.aam5690

Marchetti, C., Hobbs, J., Somkuti, P., & Laughner, J. L. (2025). A study on inferring daytime variations of from current and future space-based missions. *Earth and Space Science*, *12*(8), e2024EA003947. https://doi.org/10.1029/2024EA003947

Meijer, Y., Andersson, E., Boesch, H., Dubovik, O., Houweling, S., Landgraf, J., et al. (2023). Anthropogenic emission monitoring with the Copernicus CO_2 monitoring mission. *Frontiers in Remote Sensing*, *4*, 1217568. https://doi.org/10.3389/frsen.2023.1217568

Mitchell, K. A., Doney, S. C., & Keppel-Aleks, G. (2023). Characterizing average seasonal, synoptic, and finer variability in orbiting carbon Observatory-2 XCO2 across North America and adjacent ocean basins. *Journal of Geophysical Research: Atmospheres*, *128*(3), e2022JD036696. https://doi.org/10.1029/2022JD036696

Moore, B., III., Crowell, S. M. R., Rayner, P. J., Kumer, J., O'Dell, C. W., O'Brien, D., et al. (2018). The potential of the geostationary carbon cycle observatory (GeoCarb) to provide multi-scale constraints on the carbon cycle in the Americas. *Frontiers in Environmental Science*, *6*, 109. https://doi.org/10.3389/fenvs.2018.00109

O'Dell, C. W., Eldering, A., Wennberg, P. O., Crisp, D., Gunson, M. R., Fisher, B., et al. (2018). Improved retrievals of carbon dioxide from orbiting carbon Observatory-2 with the version 8 ACOS algorithm. *Amt*, *11*(12), 6539–6576. https://doi.org/10.5194/amt-11-6539-2018

21698996, 2026, 1, Downloaded from https://agupubs.onlinelibrary.wiley.com/doi/10.1029/2025JD044301 by Spanish Cochrane National Provision (Ministerio de Sanidad), Wiley Online Library on [03/03/2026]. See the Terms and Conditions (https://onlinelibrary.wiley.com/terms-and-conditions) on Wiley Online Library for rules of use; OA articles are governed by the applicable Creative Commons License

Olsen, S. C., & Randerson, J. T. (2004). Differences between surface and column atmospheric CO_2 and implications for carbon cycle research. *Journal of Geophysical Research*, *109*(D2), D02301. https://doi.org/10.1029/2003JD003968

Peters, W., Jacobson, A. R., Sweeney, C., Andrews, A. E., Conway, T. J., Masarie, K., et al. (2007). An atmospheric perspective on North American carbon dioxide exchange: CarbonTracker. *Proceedings of the National Academy of Sciences*, *104*(48), 18925–18930. https://doi.org/10.1073/pnas.0708986104

Riley, W. J., Biraud, S. C., Torn, M. S., Fischer, M. L., Billesbach, D. P., & Berry, J. A. (2009). Regional CO_2 and latent heat surface fluxes in the southern great plains: Measurements, modeling, and scaling. *Journal of Geophysical Research*, *114*(G4). https://doi.org/10.1029/2009JG001003

Schuh, A. E., & Jacobson, A. R. (2023). Uncertainty in parameterized convection remains a key obstacle for estimating surface fluxes of carbon dioxide. *Atmospheric Chemistry and Physics*, *23*(11), 6285–6297. https://doi.org/10.5194/acp-23-6285-2023

Taylor, T. E., Eldering, A., Merrelli, A., Kiel, M., Somkuti, P., Cheng, C., et al. (2020). OCO-3 early mission operations and initial (vEarly) XCO2 and SIF retrievals. *Remote Sensing of Environment*, *251*, 112032. https://doi.org/10.1016/j.rse.2020.112032

Taylor, T. E., O'Dell, C. W., Baker, D., Bruegge, C., Chang, A., Chapsky, L., et al. (2023). Evaluating the consistency between OCO-2 and OCO-3 XCO2 estimates derived from the NASA ACOS version 10 retrieval algorithm. *Atmospheric Measurement Techniques*, *2023*, 1–61. https://doi.org/10.5194/amt-2022-329

Torres, A. D., Keppel-Aleks, G., Doney, S. C., Fendrock, M., Luis, K., De Mazière, M., et al. (2019). A geostatistical framework for quantifying the imprint of mesoscale atmospheric transport on satellite trace gas retrievals. *Journal of Geophysical Research: Atmospheres*, *124*(17–18), 9773–9795. https://doi.org/10.1029/2018jd029933

Wagle, P., Gowda, P. H., Manjunatha, P., Northup, B. K., Rocateli, A. C., & Taghvaeian, S. (2019). Carbon and water dynamics in co-located winter wheat and canola fields in the U.S. southern great plains. *Agricultural and Forest Meteorology*, *279*, 107714. https://doi.org/10.1016/j.agrformet.2019.107714

Washenfelder, R. A., Toon, G. C., Blavier, J.-F., Yang, Z., Allen, N. T., Wennberg, P. O., et al. (2006). Carbon dioxide column abundances at the Wisconsin tall tower site. *Journal of Geophysical Research*, *111*(D22), D22305. https://doi.org/10.1029/2006JD007154

Wennberg, P. O., Roehl, C. M., Wunch, D., Toon, G. C., Blavier, J.-F., Washenfelder, R., et al. (2022). TCCON data from Park falls (US), release GGG2020.R1 (version R1) [Dataset]. *CaltechDATA*. https://doi.org/10.14291/tccon.ggg2020.parkfalls01.R1

Wennberg, P. O., Wunch, D., Roehl, C. M., Blavier, J.-F., Toon, G. C., & Allen, N. T. (2025). TCCON data from Lamont (US), release GGG2020.R1 (version R1) [Dataset]. *CaltechDATA*. https://doi.org/10.14291/tccon.ggg2020.lamont01.R1

Wunch, D., Toon, G. C., L, Blavier, J.-F., Washenfelder, R. A., Notholt, J., Connor, B. J., et al. (2011). The total carbon column observing network. *Philosophical Transactions of the Royal Society A*, *369*(1943), 2087–2112. https://doi.org/10.1098/rsta.2010.0240

Wunch, D., Toon, G. C., Wennberg, P. O., Wofsy, S. C., Stephens, B. B., Fischer, M. L., et al. (2010). Calibration of the total carbon column observing network using aircraft profile data. *Atmospheric Measurement Techniques*, *3*(5), 1351–1362. https://doi.org/10.5194/amt-3-1351-2010

Wunch, D., Wennberg, P. O., Osterman, G., Fisher, B., Naylor, B., Roehl, C. M., et al. (2017). Comparisons of the Orbiting Carbon Observatory-2 (OCO-2) XCO2 measurements with TCCON. *Atmospheric Measurement Techniques*, *10*(10), 2209–2238. https://doi.org/10.5194/amt-10-2209-2017

Wunch, D., Wennberg, P. O., Toon, G. C., Connor, B. J., Fisher, B., Osterman, G. B., et al. (2011). A method for evaluating bias in global measurements of CO_2 total columns from space. *Atmospheric Chemistry and Physics*, *11*(23), 12317–12337. https://doi.org/10.5194/acp-11-12317-2011

Yokota, T., Yoshida, Y., Eguchi, N., Ota, Y., Tanaka, T., Watanabe, H., & Maksyutov, S. (2009). Global Concentrations of CO_2 and CH_4 retrieved from GOSAT: First preliminary results. *Inside Solaris*, *5*, 160–163. https://doi.org/10.2151/sola.2009-041

21698996, 2026, 1, Downloaded from https://agupubs.onlinelibrary.wiley.com/doi/10.1029/2025JD044301 by Spanish Cochrane National Provision (Ministerio de Sanidad), Wiley Online Library on [03/03/2026]. See the Terms and Conditions (https://onlinelibrary.wiley.com/terms-and-conditions) on Wiley Online Library for rules of use; OA articles are governed by the applicable Creative Commons License